Proof-of-principle of surface detection with air-guided quantum cascade lasers

Virginie Moreau[1], Raffaele Colombelli[1], Raviv Perahia[2], Oskar Painter[2], Luke R. Wilson[3], Andrey B. Krysa[4]

[1]*Institut d'Electronique Fondamentale, Universite Paris-Sud and CNRS, UMR8622, 91405 Orsay, France*
[2]*Thomas J. Watson, Sr., Laboratory of Applied Physics, California Institute of Technology, Pasadena, California 91125, USA*
[3]*Department of Physics and Astronomy, University of Sheffield, Sheffield S3 7RH, UK*
[4]*EPSRC Centre for III-V Technology, University of Sheffield, Sheffield S3 7RH, UK*

moreau@ief.u-psud.fr

rperahia@caltech.edu

Abstract: We report a proof-of-principle of surface detection with air-guided quantum cascade lasers. Laser ridges were designed to exhibit an evanescent electromagnetic field on their top surface that can interact with material or liquids deposited on the device. We employ photoresist and common solvents to provide a demonstration of the sensor setup. We observed spectral as well as threshold currents changes as a function of the deposited material absorption curve. A simple model, supplemented by 2D numerical finite element method simulations, allows one to explain and correctly predict the experimental results.

OCIS codes: (140.5960) Semiconductor lasers; (230.5750) Resonators; (240.6680) Surface plasmons

References and links

1. F. Capasso, C. Gmachl, D. L. Sivco, and A. Y. Cho, "Quantum Cascade Lasers," Phys. Today **55**, 34 (2002).
2. J. Faist, F. Capasso, D.L. Sivco, C. Sirtori, A.L. Hutchinson, A.Y. Cho, "Quantum cascade laser," Science **264**, 553 (1994).
3. M. Beck, D. Hofstetter, T. Allen, J. Faist, U. Oesterle, M. Ilegems, E. Gini, H. Melchior, "Continuous Wave Operation of a Mid-Infrared Semiconductor Laser at Room Temperature," Science **295**, 301 (2002).
4. J. S. Yu, S. Slivken, A. Evans, L. Doris, and M. Razeghi, "High-power continuous-wave operation of a 6 μm quantum-cascade laser at room temperature," Appl. Phys. Lett. **83**, 2503 (2003).
5. M. Troccoli, D. Bour, S. Corzine, G. Hofler, A. Tandon, D. Mars, D. J. Smith, L. Diehl, and F. Capasso, "Low-threshold continuous-wave operation of quantum-cascade lasers grown by metalorganic vapor phase epitaxy," Appl. Phys. Lett. **85**, 5842 (2004).
6. L. Diehl, D. Bour, S. Corzine, J. Zhu, G. Hofler, M. Loncar, M. Troccoli, and Federico Capasso, "High-temperature continuous wave operation of strain-balanced quantum cascade lasers grown by metal organic vapor-phase epitaxy ," Appl. Phys. Lett. **89**, 81101 (2006).
7. A. Evans, S.R. Darvish, S. Slivken, J. Nguyen, Y. Bai and M. Razeghi, "Buried heterostructure quantum cascade lasers with high continuous-wave wall plug efficiency," Appl. Phys. Lett. **91**, 071101 (2007).
8. A. A. Kosterev and F. K. Tittel, "Chemical sensors based on quantum cascade lasers," IEEE J. Quantum Electron. **38**, 582, (2002).
9. C. Gmachl, F. Capasso, R. Kohler, A. Tredicucci, A. Hutchinson, D. L. Sivco, J. Baillargeon, and A. Y. Cho, "The Sense-Ability of Semiconductor Lasers," IEEE Circuits and Devices **16**, 10 (2000).
10. F.K. Tittel, Y. Bakhirkin, A.A. Kosterev. and G. Wysocki, "Recent Advances in Trace Gas Detection Using Quantum and Interband Cascade Lasers," The Review of Laser Engineering **34**, 275 (2006).

11. F. K. Tittel, D. Richter, and A. Fried, "Mid-infrared laser applications in spectroscopy," Top. Appl. Phys. **89**, 445 (2003).
12. C. Charlton, F. de Melas, A. Inberg, N. Croitoru, and B. Mizaikoff, "Hollow-waveguide gas sensing with room-temperature quantum cascade lasers," IEE Proc. Optoelectron. **150**, 306 (2003).
13. J.Z. Chen and Z. Liu and C. F. Gmachl and D. L. Sivco, "Silver halide fiber-based evanescent-wave liquid droplet sensing with room temperature mid-infrared quantum cascade lasers," Opt. Express **13**, 5953 (2005).
14. C. Charlton and A. Katzir and B. Mizaikoff, "Infrared Evanescent Field Sensing with Quantum Cascade Lasers and Planar Silver Halide Waveguides," Anal. Chem. **72**, 1645 (2000).
15. B. Lendl, J. Frank, R. Schindler, A.Muller, M. Beck, and J. Faist, "Mid-infrared quantum cascade lasers for flow injection analysis," Anal. Chem, **72**, 1645 (2000).
16. A. Edelmann, C. Ruzicka, J. Frank, B. Lendl,W. Schrenk, E. Gornik, and G. Strasser, "Towards functional group-specific detection in high-performance liquid chromatography using mid-infrared quantum cascade lasers," J. Chrom. A **934**, 123 (2001).
17. S. Schaden, M. Haberkorn, J. Frank, J. R. Baena, and B. Lendl, "Direct determination of carbon dioxide in aqueous solution using mid-infrared quantum cascade lasers," App. Spec. **58**, 667 (2004).
18. J. Faist, C. Gmachl, F. Capasso, C. Sirtori, D.L. Sivco, J.N. Baillargeon, and A.Y. Cho, "Distributed feedback quantum cascade lasers," Appl. Phys. Lett. **70**, 2670 (1997).
19. S. R. Darvish, W. Zhang, A. Evans, J. S. Yu, S. Slivken, and M. Razeghi, "High-power, continuous-wave operation of distributed-feedback quantum-cascade lasers at 7.8 μm," Appl. Phys. Lett. **89**, 251119 (2006).
20. B. G. Lee, M. A. Belkin, R. Audet, J. MacArthur, L. Diehl, C. Pflugl, F. Capasso, D. C. Oakley, D. Chapman, A. Napoleone, D. Bour, S. Corzine, G. Hofler, and J. Faist, "Widely tunable single-mode quantum cascade laser source for mid-infrared spectroscopy ," Appl. Phys. Lett. **91**, 231101 (2007).
21. L. Diehl, B. G. Lee, P. Behroozi, M. Loncar, M. A. Belkin, F. Capasso, T. Aellen, D. Hofstetter, M. Beck, and J. Faist, "Microfluidic tuning of distributed feedback quantum cascade lasers ," Opt. Express **14**, 11660 (2006).
22. S. Song, S. S. Howard, Z. Liu, A. O. Dirisu, C. F. Gmachl, and C. B. Arnold, "Mode tuning of quantum cascade lasers through optical processing of chalcogenide glass claddings," Appl. Phys. Lett. **89**, 41115 (2006).
23. P.C. Monat, P. Domachuk, and B. J. Eggleton, "Integrated optofluidics: A new river of light," Nature Photon. **1**, 106 (2007).
24. M. A. Belkin, M. Loncar, B. G. Lee, C. Pflugl, R. Audet, L. Diehl, F. Capasso, D. Bour, S. Corzine and G. Hofler, "Intra-cavity absorption spectroscopy with narrow-ridge microfluidic quantum cascade lasers," Opt. Express **15**, 11262 (2007).
25. R. Perahia, O. Painter, V. Moreau, and R. Colombelli, "Design of quantum cascade lasers for intra-cavity sensing in the mid-infrared," *in preparation*.
26. V. Moreau, M. Bahriz, R. Colombelli, R. Perahia, O. Painter, L.R. Wilson, and A.B. Krysa, "Demonstration of air-guided quantum cascade lasers without top claddings," Opt. Express **15**, 14861 (2007).
27. V. Moreau, P-A. Lemoine, M. Bahriz, Y. De Wilde, R. Colombelli, L. R.Wilson, A. B. Krysa, "Direct imaging of a laser mode via midinfrared near-field microscopy," Appl. Phys. Lett. **90**, 201114 (2007).
28. A. B. Krysa, J. S. Roberts, R. P. Green, L. R. Wilson, H. Page, M. Garcia, and J. W. Cockburn, "MOVPE-grown quantum cascade lasers operating at 9 μm wavelength," J. Cryst. Growth **272**, 682 (2004).

1. Introduction

Quantum cascade (QC) lasers are semiconductor sources that can efficiently cover the two mid-infrared (mid-IR) atmospheric windows (3 μm $\leq \lambda \leq$ 5 μm and 8 μm $\leq \lambda \leq$ 12 μm)[1]. Since their first demonstration in 1994 [2], improvements in the epitaxial growth, thermal management [3, 4, 5], and also cavity geometries have led to single mode, continuous-wave (CW) operation at room temperature at several mid-IR wavelengths [6, 7]. The use of QC lasers as monochromatic sources for chemical sensing is motivated by the fact that most molecules of chemical interest exhibit roto-vibrational transitions in the two mid-IR atmospheric windows [8, 9]. In particular, QC lasers have been applied to gas sensing [8, 10, 11, 12], but also more recently to detection in a liquid environment [13, 14, 15, 16, 17]. For detection applications, wavelength tunability is an important requirement, besides single-mode operation. Single mode operation is typically achieved using distributed feedback (DFB) technology [18], with the emission wavelength tuned by changing the heat sink temperature or the injection current. This technique yields tuning ranges of for instance 20 nm for a single device at mid-IR wavelengths [19]. Wider tuning ranges can be achieved via monolithic integration of several different DFB devices on a single chip [20]. Recently, alternative approaches have been proposed

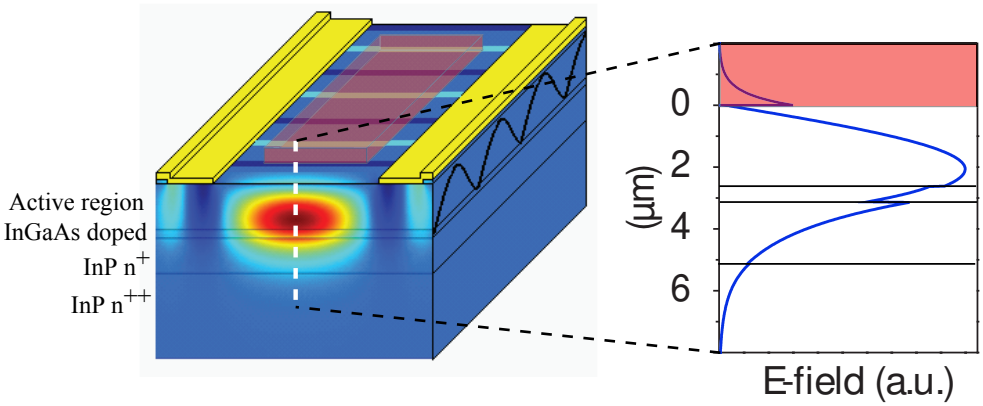

Fig. 1. Principle of surface sensing employing an air-guided QC laser. Left figure: 2D finite-element simulation of the laser mode (the magnitude of the electric field is shown) superposed onto a schematic view of the device. Right figure: 1D section of the laser mode at the center of the ridge. The orange region is the air-cladding above the device where the evanescent field penetrates, making the device sensitive to an external perturbation.

(see Refs.[21, 22]). In Ref. [22], the emission wavelength of a QC laser was tuned by photo-inducing a change of index of refraction of a chalcogenide cladding layer deposited on top of a DFB device. In Ref. [21], filling the grooves of a DFB QC laser with a material or liquid whose refractive index can be easily modified allowed fine tuning of the laser operating frequency. All the aforementioned approaches exploit the *real part* of the material/liquid refractive index in order to induce a wavelength change.

Another approach is possible however, and it consists on exploiting the *imaginary part* of the refractive index. If a laser device is engineered whose optical mode exhibits an evanescent field that penetrates in the air-claddings around the device itself, then the absorption characteristics of the external object will affect the waveguide losses, making them wavelength-dependent. The threshold current (I_{th}) and the spectral features will be both modified as a function of the material or liquid that contacts the evanescent field, thus transforming the devices in surface sensors, that could then be in principle integrated in a microfluidic chip [23].

In order to implement a surface sensor, the laser should present an evanescent field. The principle has already been demonstrated - using mid-infrared fibers - in Ref [12, 13]. One other strategy has been recently shown - using common solvents as test liquids - in Ref.[24] by Belkin et al. employing ultra-narrow ridge QC lasers. A possible alternative approach, however, is proposed in a companion article by R. Perahia et al. [25], where a surface-plasmon laser is employed with almost all the top metal cladding removed leaving only lateral contacts for current injection. These devices (which we call air-guided QC lasers) have been fabricated and characterized [26], and an aSNOM (Aperturless Scanning Near field Optical Microscopy) survey allowed the direct measurement of the evanescent field present at their surface [27].

In this paper, we show that indeed this class of devices reacts to a material or a liquid deposited on its surface, and that they are in principle suited to surface detection applications. The demonstration is corroborated by a theoretical model which is able to correctly predict the experimental results. In Section 2 the laser devices are detailed, as well as the setup used for the demonstration. In Section 3 initial results are presented and the detection principle is validated using photoresist Shipley S1818 as test material. In section 4 we give a proof of principle of fluid detection using ethanol and isopropanol as test analytes. Finally, the predicted results

obtained from a simple model will be described and they will be compared to the experimental data in Section 5.

2. Surface detection principle, device design and fabrication

Figure 1 shows the principle of surface sensing employing air-guided QC lasers. A 2D finite-elements simulation of the optical mode is superimposed onto the front facet of the laser ridge. It indicates that the mode is essentially located under the air. This characteristic yields an evanescent field, whose decay length is ≈ 500 nm as deduced from the 1D simulation of Fig. 1(b), and from experimental measurements [27]. When an absorbing material (or liquid) is deposited on such a device, the total propagation losses become frequency dependent, leading to a different transparency (and therefore emission) wavelength, and also to an increase of the current threshold. Since the details of the frequency-dependent losses depend on the absorption features of the analyte deposited on the surface, these devices can be used as sensors.

The laser heterostructure used (MR2230) was grown by low pressure (150 Torr) metal organic vapor phase epitaxy (MOVPE), using an InGaAs/AlInAs heterostructure lattice matched to a highly-doped InP substrate. Further details of the growth process can be found in [28]. The active region is based on a standard two-phonon-resonant design, and the target wavelength is $\lambda = 7.5\ \mu$m.

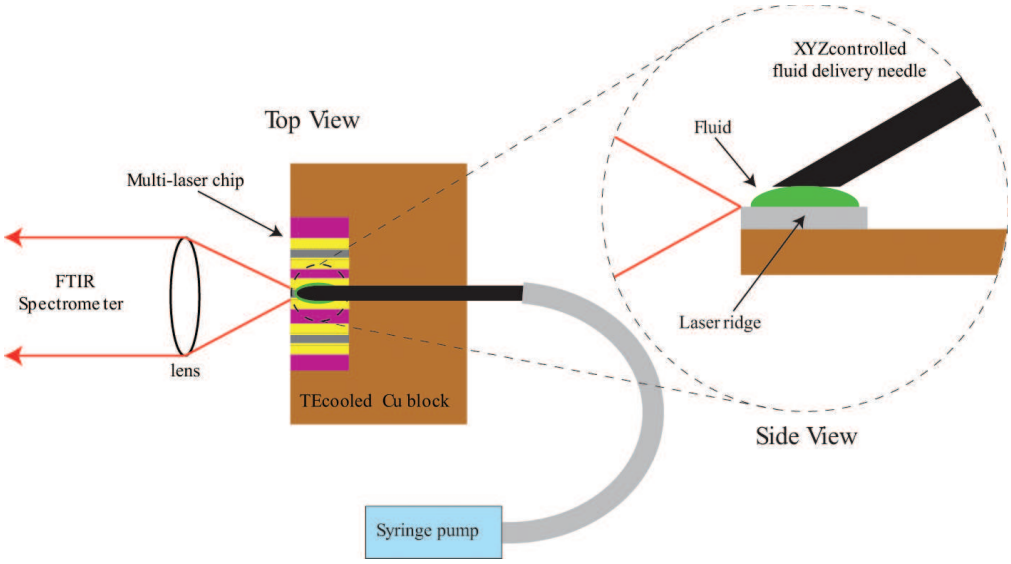

Fig. 2. Sketch of the experimental setup used for the measurements. The laser devices are soldered with indium on a copper block. This latter is then mounted onto a Peltier-Cooler. (a) Side view. (b) Top view. The emitted light is collected from the laser facet and fed into a FTIR spectrometer operated in rapid-scan mode, with a typical resolution of 0.125 cm^{-1}. A liquid-nitrogen-cooled MCT detector was used.

The lasers are fabricated in a standard ridge mesa etched (26-31-36-41 μm-wide) Fabry-Perot cavity configuration. Most of the device top surface is left exposed, and the electrical current is injected through lateral metallic contacts (Ti/Au, 30/300 nm) located on the two sides of the resonators. In Fig. 1(a) the lateral contacts are schematically represented in yellow. Details of the samples and of their operating characteristics are reported in Ref. [26]. After mechanical polishing and back contact deposition, the samples were cleaved into laser bars of typically 1.5

mm length, mounted with indium solder on copper blocks, wire-bonded and characterized on a Peltier holder.

Laser spectra and light-current (LI) characteristics, and the absorption curves of the investigated test liquids (ethanol and isopropanol) were all taken using a Fourier Transform Infrared Spectrometer. Shipley resist S1818, isopropanol (IPA) and ethanol have been employed to provide a proof-of-principle of the operation of the devices as sensors. A scheme of our setup for fluid delivery is shown in Fig. 2. To control the stability of a drop of liquid on the device top surface, we used a bevel shaped needle and a push-syringe. At a certain, specific pushing speed, the fluid delivery is compensated by its evaporation and the drop is stable in volume. Two CCD cameras are used for real-time control of the fluid delivery on the samples. Before sensing tests, the devices were measured as reference.

3. Surface sensitivity: photoresist detection

In order to demonstrate the surface-sensitivity of the devices, Shipley photoresist (S1818) was used as test absorbing analyte. We chose photoresist for the following reasons: first, it is well known that resist exhibits strong absorption features at mid-IR wavelengths (see Fig. 3). Secondly, it is relatively straightforward to deposit it with precision on top of the lasers using photolithographic techniques.

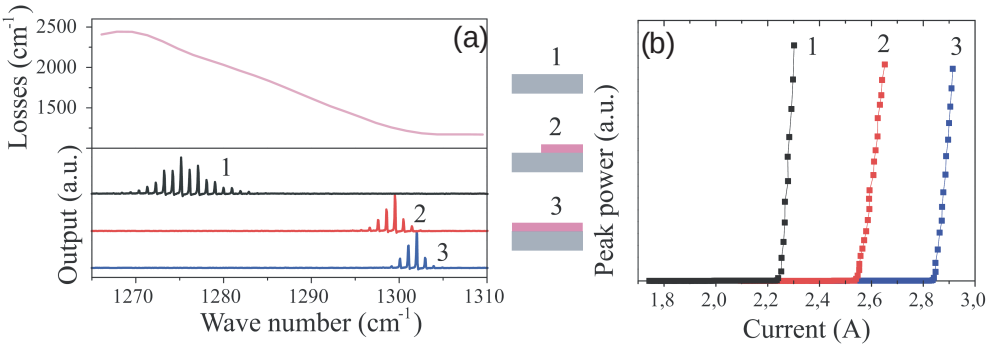

Fig. 3. (a) Laser tuning upon S1818 photoresist deposition on the device top surface. Black curve: emission spectrum of the laser device before resist deposition. Blue curve: emission spectrum with the resist deposited on the top surface. Red curve: emission spectrum with the resist deposited on half the top surface. Purple curve: calibrated absorption spectrum of Shipley photoresist S1818, obtained via FTIR spectroscopy. The lasers were typically operated with 50-ns-wide pulses at a repetition rate of 84 kHz. (b) Light-current-voltage (LIV) curve of the device without and with resist. The current threshold of the unperturbed device (black curve) is approximately 27% lower than the threshold when the resist is deposited on the surface (blue curve). When the resist is deposited on half the top surface (red curve) the threshold approximately 13% higher than the unperturbed case. The lasers were operated with 50-ns-wide pulses at 84 kHz repetition rate.

The resist was spun onto laser devices already mounted on a copper block in order to have them previously tested. Selective sample exposition to UV light and development allows one to completely remove the resist from the copper block and from the sample facets, until the resist covers the top device surface only. Care was taken in order to completely remove the resist from the laser facets. Figure 3 shows the results obtained from a 41-μm-wide laser ridge. A global frequency blue-shift of the laser spectral envelope of ≈ 27 cm^{-1} (Fig. 3(a)), and an

increase of nearly 27% in the threshold current have been observed (Fig. 3(b)). The absorption curve of the resist used for the test (Shipley S1818) - as obtained with FTIR spectroscopy - is reported in Fig. 3(a). It presents a linear behavior with a negative differential absorption around the emission frequency of the laser. We expect therefore that the transparency condition will be reached at shorter wavelengths when the resist is deposited on the device top surface, since the analyte losses decrease with an increase in frequency. This prediction is correctly confirmed by the experiment. Furthermore, the resist deposition on the device top surface increases the total propagation losses, and the expected increase of I_{th} has been correctly observed experimentally. In addition, when only half of the device surface is covered with resist the I_{th} increase is only 13%, proving that it scales linearly with the volume of absorbing material probed. The laser spectral envelope shift is in this case ≈ 25 cm^{-1}. As a final check, the photoresist was removed with acetone and the devices were re-tested: emission frequency and I_{th} were the same as the values obtained prior to resist deposition.

4. Surface sensitivity: discrimination between two test liquids

The goal of this section is to investigate if monitoring the variations of the emission frequency and/or of the current threshold of the lasers we developed allows one to discriminate between two test chemicals. We chose to test the devices with isopropanol (IPA), ethanol and a mixture of both (50% IPA-50 % ethanol). The reason for this choice is the reasonably strong absorption exhibited by both the analytes in the 7.5 μm $\leq \lambda \leq$ 8 μm spectral range of interest (see Fig. 4). Upon fluid deposition (with the technique described in Fig. 2), we observe two clearly distinguishable spectral effects: a global frequency shift of the laser envelope of Fabry-Perot modes (accompanied by a small change of the mode spacing), as well as an increase of the laser threshold current.

Figure 4(a) reports the spectral characteristics of a 41-μm-wide air-guided QC laser upon deposition of IPA and ethanol, respectively. The black curves represent the laser emission when no liquid is present. When IPA (ethanol) is deposited on the top surface, the envelope of the laser emission tunes from 1275 cm^{-1} to 1270 (1285) cm^{-1}, respectively. The measured absorption spectra of the two solvents are reported in Fig. 4(a) (red and blue curves). A comparison with the spectra demonstrates that the laser tunes its emission frequency in order to minimize the propagation losses, that are modified by the presence of the fluid on the top surface. It must be noted that ethanol shows a nearly symmetric absorption peak at a frequency of 1275 cm^{-1}. A blue-shift as well as a red-shif can therefore be expected. However, free carrier absorption must be taken into account. Since its magnitude scales approximately as λ^2, a blue-shift to higher frequencies minimizes the losses, and it can explain what we indeed observe experimentally.

These results show that the spectral changes of the devices upon liquid deposition allow one to discriminate *pure* IPA from *pure* ethanol. One can wonder if a dilution of the two liquids can also be detected with the same system. Upon deposition of a 50%-50% mixed solution of IPA and ethanol, an intermediate spectral behavior was in fact observed as shown in Fig. 4(b). We can approximately estimate the volume of liquid which can interact with the device near field. The typical device has an air-gap opening of 24 μm. For a 1.5 mm long laser, and considering that the evanescent field extends for 0.5 μm above the sample surface, we obtain a volume $\approx$18 pL. This value represents an estimate for the volume of liquid which is, in principle, sufficient for sensing with the proposed technique. A slightly better value of 10 pL is estimated for the devices proposed in Ref. [24]. However, it is important to note that prior knowledge of the absorption spectra of the analyzed material/liquid is necessary. At this stage therefore, this system can be used to detect a certain known chemical after pre-calibration, but not to detect unknown species, nor to obtain a quantitative measurement of the analyte dilution in a liquid.

As for the effect on the laser threshold, upon IPA, ethanol, and 50 %-50 % dilution deposi-

tion, I_{th} increased by 10.6 %, 10.6 %, and 11.45 %, respectively. The threshold current cannot therefore be considered a discriminating parameter since almost identical increases have been obtained for IPA and for the 50 %-50 % dilution. This finding indicates that the detectivity of the system is rather limited. The two solvents absorption at a frequency corresponding to the laser emission are 315 cm^{-1} for IPA and 404 cm^{-1} for ethanol, respectively, while the S1818 resist absorption at the same frequency is 716 cm^{-1}, i.e. approximately two times larger. It appears therefore that this system could be used as a detector - by monitoring I_{th} upon liquid deposition - if the absorption magnitudes differ by few hundreds of cm^{-1}.

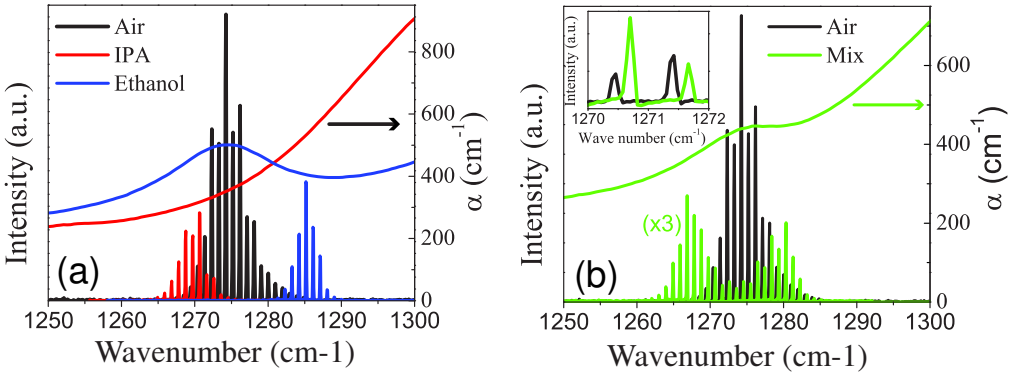

Fig. 4. (a) Laser tuning of a 41-μm-wide air-guided QC laser upon ethanol (blue spectrum) and IPA (red spectrum) deposition. The black spectrum represents the unperturbed laser emission. The red (blue) curves represent the measured absorption of IPA and ethanol, respectively. The measurements were taken at 18 C degrees. The lasers were operated at 84 kHz, with 50-ns-wide pulses. The signal was fed into an FTIR spectrometer and detected with an MCT detector. (b) Laser tuning with a 50%-50% mixed solution of IPA and ethanol (green spectrum). The green curve represents the measured absorption of the solution. Inset: frequency shift of the Fabry-Perot mode spacing upon fluid deposition. Black curve: without fluid. Green curve: with fluid.

5. Theoretical model and discussion

In order to explain the experimental results, we introduce a theoretical model that allows one to write a simple expression for the total losses in the presence of an absorbing material (or liquid) in the device near field. By imposing the transparency condition (i.e. total losses equal to gain), we can obtain the laser emission frequency shift in the presence of the absorber on the device surface. A full theoretical model is developed and discussed in a separate paper [25].

The laser material gain is modeled as a Lorentzian function centered at ν_g, with a full width at half maximum (FWHM) of 130 cm^{-1}($\approx$10% of the central frequency). The total propagation losses per unit length of the laser are described as the sum of two contributions: waveguide (α_{wg}) and mirror (α_m) losses. The frequency dependence of the waveguide losses is assumed to be dominated by free carrier absorption, and it is taken into account by adding a dependence proportional to ν^{-2} and to α_{wg} calculated at a fixed frequency ν_0. This is in general a good approximation. The presence of the liquid in the near field of the laser is taken into account via its complex index of refraction $n_a = n0 + ik_a$ through first order perturbation theory of Maxwell's equations. The index real part $n0$ induces a minor shift of the laser frequency (see inset of Fig. 3(b)), while its imaginary part k_a induces - to first order - an increase in laser threshold. It can be shown in fact that the waveguide loss perturbation is proportional to the

product $\Gamma_e k_a$, and therefore to $\Gamma_e \alpha_a$ (where α_a is the analyte absorption and Γ_e is the percentage of energy of the evanescent mode)[25]. Furthermore, a frequency-dependent loss will modify the transparency condition and it will produce a shift of the laser frequency as well. The shift can be actually much larger than the very small one induced by the real part only of the index of refraction. It is exactly this phenomenon that can successfully explain the experimental results.

Within this model, the total losses at a frequency ν - when an absorber is present in the laser near field - can be expressed as follows [25]:

$$\alpha_{total}(\nu) = \alpha_m + \alpha_{wg}(\nu_0)(\frac{\nu_0}{\nu})^2 + \frac{n_g}{n_0}\Gamma_e \alpha_a(\nu), \quad (1)$$

where n_g is the modal group index.

An extremely simplified linear approximation for the wavelength-dependent analyte absorption close to the peak laser gain yields an intuitive view of the mechanism on which the sensor is based. With a typical absorption a 500 cm^{-1} (corresponding to the absorption value of ethanol or isopropanol at a wavelength $\lambda \approx 7.5$ μm), we found that two liquids deposited on the same laser device can be distinguished if (i) the magnitudes of their absorption are different and/or (ii) if their differential absorption (defined as $\partial\alpha/\partial\nu$, where ν is the frequency) have opposite signs. In addition, the frequency shift depends on the initial laser emission frequency ν_g, defined as the emission frequency of the unperturbed laser. This system seems therefore able to distinguish between two different absorbing materials (or liquids). The laser threshold current (I_{th}) is another relevant parameter, which depends only on the loss magnitude at the peak laser gain. As a consequence, two different chemicals can be discriminated on the basis of their effect on I_{th} only if their absorptions are different enough. No effect on the other hand is expected on I_{th} if just a difference in the differential absorption is present.

In order to go beyond this very simple linear approximation, we introduced in the model the real absorbing curves of the solvents used for the experiment. This allows one to obtain a more accurate modeling of the the behavior of the air-confined lasers in presence of absorbing liquids, and to predict the laser frequency shift upon fluid deposition. The values for $\alpha_{wg}(\nu_0)$, Γ_e and n_g are obtained numerically with 2D finite elements simulations, while ν_g is assumed to be the emission frequency of the unperturbed laser. The table below summarizes the parameters employed in the simulation:

FHWM (cm^{-1})	ν_g (cm^{-1})	ν_0 (cm^{-1})	$\alpha_{wg}(\nu_0)$ (cm^{-1})	n_0	n_g	Γ_e (%)	R	L (cm)
130	1275	1300	9.03	1.4	3.25	0.192	0.28	0.15

The lasing threshold condition - gain equals loss - is then used to relate the loss introduced by the absorber to the lasing frequency and to its threshold current density.

The theoretical results obtained by applying the model to the tested laser devices are shown in Fig. 5, together with a summary of the experimental results. The bottom part of panel (a) reports the emission spectra of the laser devices in the unperturbed case (black curve), and upon IPA (red curve) and ethanol (blue curve) deposition, respectively. A global shift of the spectral envelope is clearly observable. The top part of panel (a) reports instead a visual representation of the lasing threshold condition in the presence of IPA (red curves) or ethanol (blue curves). The full lines represent the total losses in the presence of the analyte, as obtained from Eq. 1. The dashed lines represent the material gain at transparency: the tangential condition identifies the predicted laser frequencies (vertical full lines), which are found in good agreement with the experimental findings.

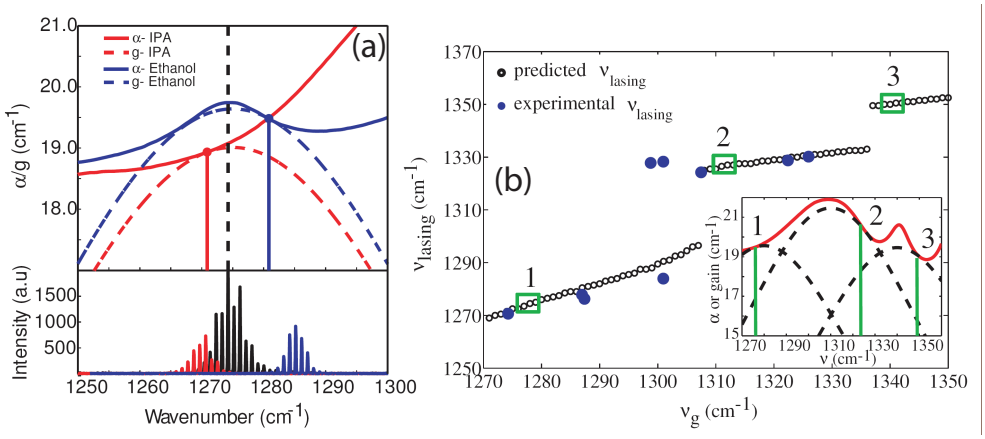

Fig. 5. (a) Absorption model (b) Experimental (blue circle) vs. predicted (black circle) lasing frequencies for IPA as a function of initial frequency. Inset shows lasing condition for three characteristic initial frequencies

The experiments have been performed on several laser devices, each having a different initial emission frequency thanks to the inherent variability of processing, semiconductor wafer non-uniformity, etc... All the results - in the case of IPA detection - are reported in Fig. 5(b): ν_g is the initial, unperturbed laser emission frequency, and ν_{lasing} is the emission frequency when IPA is present in the device near-field. The black circles represent the prediction of the theoretical model, while the blue circles correspond to the experimental results. The agreement between theory and experiment is good, and it shows that the model indeed allows one to predict the laser behavior upon fluid deposition, and to discriminate - in this case - IPA from ethanol. Furthermore, the inset of Fig. 5(b) reports a visual representation of the lasing threshold condition for three characteristic initial laser frequencies ν_g, marked by the green rectangles in the main panel. It provides a direct, intuitive explanation for the presence of ”jumps” in the predicted as well as in the experimental curves, and it further confirms that the proposed theoretical model can successfully predict the behavior of these surface sensors.

As for the current threshold, the model predicts an increase of 10.7% of I_{th} when IPA is deposited, and of 12.37% when ethanol is deposited, while the experiment yields and increase of I_{th} by 10.6% in both cases. The agreement between theory and experiment is fair. The small discrepancy between the predicted and experimental result for ethanol could originate from the confinement factor (Γ), which is modified by the presence of the fluid on the device top surface. We employed Γ = 73.9% for the unperturbed laser, and Γ = 74.5% in the presence of both ethanol and IPA. A better approximation would take into account their slightly different indeces of refraction, yielding different confinement factors.

6. Conclusions

In this initial work, we have demonstrated that mid-infrared QC lasers featuring air-guided waveguides (a relatively straightforward architecture from a technological point of view) are suited to surface sensing of liquids with absorption features close to the laser emission frequency. In particular, we provided a simple theoretical model that correctly predicts the spectral and threshold behavior of the lasers when an absorbing material or liquid is present in the device near-field. These results are promising for optofluidics application. For instance, if I_{th} only needs to be monitored, the system would consist of the QC laser (and its microfluidic chip), and

a detector which could even be integrated on the chip itself, employing for instance the same quantum cascade structure in a photo-current configuration. However, the drawback is that - in the current configuration - the absorption curves of the liquid to be detected need to be known in advance.

Finally, these devices present some disadvantages. Their emission is not single mode, the central emission frequency is hardly predictable, their sensitivity is rather limited, and their integration on a microfluidic chip is complicated by their lack of planarity. A new device geometry, which can solve the aforementioned problems, is based on micro-cylindrical resonators, it has been studied, and the results are presented in a companion article [25]. The results of the analysis suggest that micro-cylindrical devices will exhibit improved sensitivity to the presence of an absorbing liquid in their near-field. In addition, they can be implemented as arrays of single mode micro-lasers on the same chip, an ideal geometry for the fabrication of a microfluidic circuit. These new devices, once developed, will allow to assess if this sensing approach can measure in an analytically relevant concentration range, an assessment that was not possible with the current device architecture.

Acknowledgments

This work was conducted as part of a EURYI scheme award (www.esf.org/euryi). The Caltech portion of this work was supported by the DARPA Center for Optofluidics (http://www.optofluidics.caltech.edu). This work is supported by the UK Engineering and Physical Sciences Research Council (EPSRC) and by the Royal Society. The device fabrication has been performed at the nano-center “Centrale Technologique Minerve” at the Institut d’Electronique Fondamentale.